

Modeling and Direct Simulation of Velocity Fluctuations and Particle-Velocity Correlations in Sedimentation

F. R. Cunha

G. C. Abade

A. J. Sousa

Department of Mechanical Engineering,
University of Brasília,
Campus Universitário,
70910-900 Brasília-DF, Brazil

E. J. Hinch

Department of Applied Mathematics
and Theoretical Physics,
University of Cambridge,
Silver Street,
Cambridge CB3 9EW, UK

In this paper we present direct numerical simulations of monodisperse and polydisperse suspensions of non-Brownian particles sedimenting at low Reynolds number. We describe a scheme to generate ergodic ensembles of random particulate systems and a numerical procedure for computing interactions among spherical particles based on Ewald summation technique for hydrodynamic mobility tensors. From the generation process truly random both monodisperse and multimodal size distributions of particles were obtained for dilute and moderate densities based on a minimum energy criterion. Concerned with computations of the Ewald sums our numerical procedure drastically reduces the CPU simulation time providing results of the hindered settling function in good agreement with available experimental data and asymptotic results for ordered and random periodic arrays of particles. We show new computer simulations with no flux boundary perpendicular to gravity and periodic boundary conditions in horizontal direction. The simulations reproduce the experimental correlation-time and anisotropy of the velocity fluctuations, but have the magnitude of these fluctuations increasing proportional to the size of the system. [DOI: 10.1115/1.1502665]

1 Introduction

The sedimentation of solid particles in a viscous fluid is a common industrial process in civil, chemical, and oil engineering. Much theoretical and experimental research has been directed at determining the sedimentation velocity for monodisperse suspensions, [1]. The most popular result is the simple formula of Richardson and Zaki [2]: $\langle U \rangle = U_0(1 - \phi)^n$, where $U_0 = 2\Delta\rho a^2 g / 9\mu$ is the Stokes velocity for an isolated particle, a is the particle radius, $\Delta\rho$ denotes the difference between the density of the solid particles and fluid, μ is the fluid viscosity, g is the acceleration due to gravity, and $n = 5.1$ for spherical particles with low Reynolds numbers. On the theoretical side, the origin, significance, and interpretation of the convergence difficulties in calculating the sedimentation velocity are well understood after the rigorous theories of Batchelor [3,4] for predicting sedimentation velocities in monodisperse and polydisperse dilute suspensions of spheres at low Reynolds number. On the other hand the problem of velocity fluctuations in sedimentation is still unresolved theoretically, [5,6]. Theories, [7–13], and numerical computations, [14–17], with randomly positioned monodisperse particles find that fluctuations diverge with increasing system size. Most experiments find differently, [18,19].

The first theoretical work to investigate the convergence problem of the rms fluctuations in sedimentation was developed by Caffisch and Luke [7], who pointed out that Batchelor's renormalization does not resolve the divergence associated with calculating the variance of the sedimentation velocity. A physical scaling argument based on buoyancy-driven convection in sedimentation was given by Hinch [8]. The scalings confirmed the predictions of Caffisch and Luke. Koch [10] has adapted Hinch's scalings to gas-solid suspensions and studied the behavior of fluctuations in a range of moderate particle Stokes numbers, $1 \ll \text{St} \ll \phi^{-3/4}$. Several theoretical approaches have attempted to explain the fluctua-

tion screening in sedimentation. Koch and Shaqfeh [9] argued that screening of the velocity fluctuations results from correlations in the particle distribution. The distribution is characterized by a net deficit of exactly one particle surrounding any test particle. This theory predicts that the velocity fluctuations scale like U_0 , independent of the solid volume fraction ϕ , and that the correlation length scales as $a\phi^{-1}$, in contrast to the experiments carried out by Segré, Herbolzheimer, and Chaikin [19] and Guazzelli [6] who found velocity fluctuations of order $U_0\phi^{1/3}$ and correlation length of order $10a\phi^{-1/3}$. Recently, Brenner [13] has examined through scaling and numerical simulations the effect of side walls on arguments leading to the prediction of diverging velocity fluctuations with container size. The analysis has not definitively explained the dependence of the velocity fluctuations on the size of the settling box, although it seems to predict a divergence weaker than Caffisch-Luke theory. Dynamical simulations of sedimenting particles with point particles approximation or full hydrodynamic interaction in periodic systems, and large-scale lattice-Boltzmann numerical simulations support the conclusion, finding an increase in the magnitude of the velocity fluctuations and hydrodynamic diffusivity with the size of the numerical box, [14–17,20].

Several experiments have also been carried out to investigate fluctuations in sedimentation. Davis and Hassen [21] examined the spreading of the interface at the top of a sedimenting, slightly polydisperse suspension of non-Brownian particles. An investigation of the simultaneous effects of self-sharpening and velocity fluctuations in a sedimenting suspension of noncolloidal particles has been made by Lee et al. [22]. Ham and Homsy [23] carried out experiments to investigate the nature of the motion of a test particle sedimenting in the midst of a suspension of like particles. Their experiments found that fluctuations in the sedimentation velocity over relatively short settling distances are large (ranging from 25% to 46% of the mean) with dimensionless self-dispersion coefficients parallel to gravity increasing from approximately $2aU_0$ at $\phi = 25\%$ to $6aU_0$ at $\phi = 5\%$, which is about a factor of 5 smaller than the gradient diffusivity reported by Lee et al. [22]. Using a multiple light scattering technique, Xue et al. [24] measured the effects of hydrodynamic interactions on the average

Contributed by the Fluids Engineering Division for publication in the JOURNAL OF FLUIDS ENGINEERING. Manuscript received by the Fluids Engineering Division April 21, 2000; revised manuscript received April 30, 2002. Associate Editor: L. A. Mondy.

sedimentation velocity, its variance and the short-time self-diffusion coefficient in a concentrated hard-sphere colloidal suspension. Important experiments in sedimentation were carried out by Nicolai et al. [25], who have also investigated velocity fluctuations in a monodisperse sedimenting suspension of spheres under conditions of low Reynolds number. These experiments estimated velocity fluctuations between 75% and 170% of the mean, larger than those of Ham and Homay [23]. In addition they observed a strong anisotropy in the velocity fluctuations and self-diffusivities, $D_{\parallel}/D_{\perp} \approx 5$ at 5%, although substantially smaller than that found by the theory of Koch [14] and numerical simulations of Ladd [15,16]. The indices \perp and \parallel denote quantities parallel and perpendicular to gravity. At moderate concentration, Nicolai and Guazzelli [18] found differently from the theories and computations that particle velocity fluctuations and hydrodynamic self-dispersion coefficients did not depend on the container dimension as the inner width of the vessel varied by a factor of four. The experiments, [18], unfortunately disagree with the theoretical predictions. This contrary result may be an indication that a well mixed particle distribution cannot, in principle, remain unchanged during sedimentation, and that information about the evolution of the microstructure in time is required to understand the behavior of the velocity fluctuations. We argue that after the suspension evolves the strong convection current observed in the initial stages of sedimentation will remove horizontal fluctuations in the number density leading to a saturation of velocity fluctuations. We should also mention here the related phenomenon of shear-induced hydrodynamic diffusion in sheared suspensions, [26,27].

The objective of this paper is to investigate by computer simulation the average sedimentation velocity, the particle velocity fluctuations, and particle-velocity correlations during sedimentation. We examine monodisperse and bidisperse suspensions with randomly positioned particles for different volume fractions and size of the container. In Section 2 we will present scaling arguments for velocity fluctuations and dispersion in sedimentation. The basic method is presented in Section 3 where we describe in detail both the calculation of the far-field interactions and short-range interactions for closing particles. In Section 4 the numerical scheme for polydisperse suspensions will be explained. This computational scheme will then be tested in Section 5 by comparing results of sedimentation velocity for ordered and random suspensions with analytical predictions and Richardson-Zaki empirical correlation. Simulation results for monodisperse and bidisperse sedimentation are presented. Conclusions will be stated in Section 6.

2 Scalings

One can begin to understand the scaling of the velocity fluctuations by considering a box of size l containing N particles distributed uniformly, with the number of particles related to the size of the box and the volume fraction ϕ by $N = l^3 \phi / \frac{4}{3} \pi a^3$. If the box is divided into two equal parts by a vertical plane, due to statistical fluctuations one half of the box will typically contain $N/2 + \sqrt{N}$ particles, whereas the other half will contain $N/2 - \sqrt{N}$. This imbalance drives convection currents during the sedimentation process. The extra weight on the heavy side is $mg\sqrt{N}$, with $m = \frac{4}{3} \pi a^3 \Delta \rho$. Balancing this fluctuation in weight with a Stokes drag $6\pi\mu U'l$ on the velocity fluctuation, and using $U_0 = 2\Delta\rho a^2 g / 9\mu$, we find the fluctuation in the velocities.

$$U'^2 \sim U_0^2 \phi \frac{l}{a} \quad (1)$$

With this velocity fluctuation we can estimate the hydrodynamic self-diffusivity as $D \sim U'l$, corresponding to the particle velocity remaining correlated for a time $\tau_c = O(l/U')$. Thus

$$D \sim a U_0 \phi^{1/2} \left(\frac{l}{a} \right)^{3/2}. \quad (2)$$

This scaling argument helps to explain how velocity fluctuations and hydrodynamic self-diffusivity in a random dilute sedimenting suspension depend on the size of the system.

In the simulations we shall be monitoring the horizontal variation of density which is responsible for the convection currents in sedimentation. This is the important origin of the large velocity fluctuations which has not been made clear by previous works who have worried about Koch and Shaqfeh's mass deficit theory, [9].

3 Statement of the Problem

Consider a suspension of N rigid and spherical particles interacting hydrodynamically. The spheres differ in radius and density. The particulate dispersion is subject to a sedimentation process through a Newtonian fluid of viscosity μ and density ρ_f with low-Reynolds-number flow about each particle. The system occupies a three-dimensional unit cell represented by a prismatic container with dimensions $d \times l \times h$. In order to simulate an infinite suspension, the unit cells comprise a periodic spatial structure like a Bravais lattice (see Fig. 1).

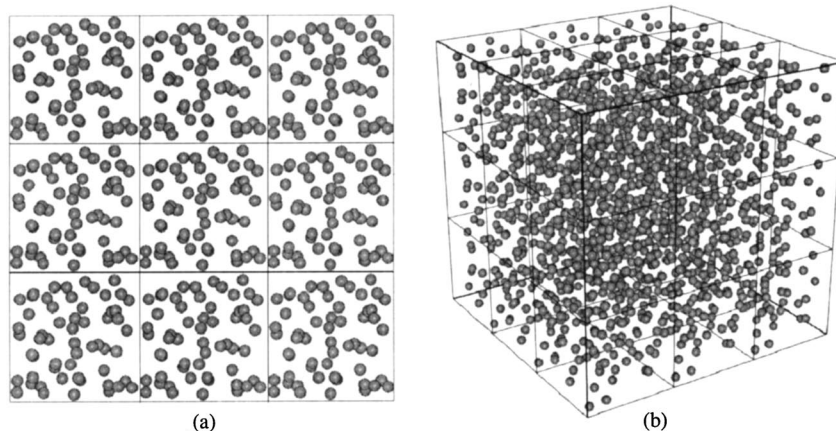


Fig. 1 Representation of a typical lattice used in the simulations. The particles are randomly distributed in a periodic cell with $\phi=0.03$. (a) Side view; (b) three-dimensional perspective view.

In the case in which the particulate phase consists of m species of particles, one follows an usual notation and denotes, respectively, the radius, density, number density, and volume fraction of each particle of species s by a_s , ρ_s , n_s , and ϕ_s . The dimensionless polydispersity parameters concerned with species s will be denoted by aspect ratios λ_s and reduced density ratios η_s as follows:

$$\lambda_s = \frac{a_s}{a}, \quad \eta_s = \frac{\rho_s - \rho_f}{\rho - \rho_f}, \quad (s=1, 2, \dots, m), \quad (3)$$

where a and ρ correspond, respectively, to the characteristic radius and density of the species adopted as the reference for non-dimensionalization purposes. The other species are expressed in terms of the parameters λ and η . Thus, the terminal settling velocity of an isolated particle, the Stokes-Einstein diffusivity and the Péclet number of species s are, respectively,

$$\mathbf{U}_0^{(s)} = \eta_s \lambda_s^2 \mathbf{U}_0, \quad D_0^{(s)} = \lambda_s^{-1} D_0, \quad \text{Pe}^{(s)} = \eta_s \lambda_s^2 \text{Pe}_0, \quad (s=1, \dots, m) \quad (4)$$

where

$$\mathbf{U}_0 = \frac{2}{9\mu} a^2 (\rho - \rho_f) \mathbf{g}, \quad D_0 = \frac{\kappa T}{6\pi\mu a}, \quad \text{Pe}_0 = \frac{aU_0}{D_0}, \quad (5)$$

\mathbf{g} is the gravitational force per unit mass, κ is the Boltzmann constant and T is the absolute temperature. The length quantities are made nondimensional using a as the characteristic length scale. The Stokes hydrodynamic drag $6\pi\mu a U_0$ is taken as the characteristic reference scale for force.

3.1 Lattice Sums. In view of the well-known convergence problem inherent in the long-range nature of the hydrodynamic interaction, one adopts a formulation based on the Beenakker's Ewald-summed Rotne-Prager tensor, [28–30], under the assumption that pairwise additivity of the hydrodynamic interaction is plausible at dilute conditions. An extension of the formulation proposed by Beenakker for hydrodynamic interactions in a heterogeneous suspension and some basic background information about the periodic array in space are presented next.

Let the center positions of the N spheres within a unit cell be denoted by the set of vectors $\mathcal{C}_N = (\mathbf{x}_1, \dots, \mathbf{x}_N)$. Consider a periodic lattice in which the set \mathcal{C}_N assumes the general form $\mathcal{C}_N = (\mathbf{x}_{\gamma 1}, \dots, \mathbf{x}_{\gamma N}) = (\mathbf{x}_1 + \mathbf{x}_\gamma, \dots, \mathbf{x}_N + \mathbf{x}_\gamma)$ where

$$\mathbf{x}_\gamma = (\gamma_1 d, \gamma_2 l, \gamma_3 h), \quad (\gamma_1, \gamma_2, \gamma_3 = 0, \pm 1, \pm 2, \dots) \quad (6)$$

defines the lattice points, obtained by a linear combination of the basic orthogonal vectors $d\mathbf{e}_1, l\mathbf{e}_2, h\mathbf{e}_3$, $\gamma = \{\gamma_1, \gamma_2, \gamma_3\}$ being the set of integer coefficients, named the cell indices, and the set of vectors $\{\mathbf{e}_1, \mathbf{e}_2, \mathbf{e}_3\}$ being the canonical base of the Euclidian space.

The reciprocal lattice vectors \mathbf{k}_ζ specifies lattice waves satisfying the periodic boundary condition. Thus the function $e^{i\mathbf{k}_\zeta \cdot \mathbf{x}_\gamma}$ is periodic with respect to the basic vectors and assumes a unit value for all $\gamma \in \mathbb{Z}$. The vectors \mathbf{k}_ζ have the dimension of the inverse of length and are written as

$$\mathbf{k}_\zeta = 2\pi \left(\frac{\zeta_1}{d}, \frac{\zeta_2}{l}, \frac{\zeta_3}{h} \right), \quad (\zeta_1, \zeta_2, \zeta_3 = 0, \pm 1, \pm 2, \dots) \quad (7)$$

where $\zeta = \{\zeta_1, \zeta_2, \zeta_3\}$ is the cell index of the reciprocal lattice.

The evaluation of the sedimentation velocity \mathbf{U}^α of a test particle (numbered by the index α) considering the flow disturbances induced by the neighboring ones involves the computation of two mobility matrices. The first matrix is relative to an isolated particle being represented by an isotropic tensor. The second one consists of a two-sphere mobility which considers the particle images periodically replicated. The last mobility includes terms with respect to the lattice sums in real and reciprocal space, being the sums convergence rate controlled by a positive parameter ξ . One attributes to the convergence parameter a value ξ

$= \pi^{1/2} V^{-1/3}$ suggested by Beenakker [28] as a good choice in the case of a simple cubic lattice, where V denotes the volume of the unit cell.

Now, consider an arbitrary pair of particles numbered by the indices α and β , pertaining to species s and p , respectively. The velocity of a particle α is given by

$$\mathbf{U}^\alpha = \mathbf{M}^\alpha \cdot \mathbf{F}^\alpha + \sum_{\substack{\gamma \\ \mathbf{x}_{\gamma\beta} \neq \mathbf{x}_\alpha}} \sum_{\beta=1}^N \mathbf{M}^{(p,s)}(\mathbf{x}_{\gamma\beta} - \mathbf{x}_\alpha) \cdot \mathbf{F}^\beta + \frac{1}{V} \sum_{\substack{\zeta \\ \mathbf{k}_\zeta \neq 0}} \sum_{\beta=1}^N \mathbf{M}^{(r,s)}(\mathbf{k}_\zeta) \cdot \mathbf{F}^\beta \cos[\mathbf{k}_\zeta \cdot (\mathbf{x}_\beta - \mathbf{x}_\alpha)], \quad (8)$$

where

$$\mathbf{M}^\alpha = \left(1 - 6\xi \pi^{-1/2} - \frac{40}{3} \pi^{-1/2} \xi^3 \right) \mathbf{I}. \quad (9)$$

\mathbf{M}^α defines the α th isolated particle mobility and \mathbf{I} denotes the unit second rank tensor. The periodic two-sphere mobilities are defined by the following expressions:

$$\begin{aligned} \mathbf{M}^{(p,s)}(\mathbf{r}) = & \left\{ 3\xi^3 r^2 - \frac{9}{2}\xi + (4\xi^7 r^4 - 20\xi^5 r^2 + 14\xi^3 \right. \\ & \left. + \xi r^{-2}) \lambda \right\} \pi^{-1/2} \exp(-\xi^2 r^2) + \left(\frac{3}{4} r^{-1} + \frac{1}{2} r^{-3} \lambda \right) \\ & \times \text{erfc}(\xi r) \left\{ \left[-3\xi^3 r^2 + \frac{3}{2}\xi + (-4\xi^7 r^4 \right. \right. \\ & \left. \left. + 16\xi^5 r^2 - 2\xi^3 - 3\xi r^{-2}) \lambda \right] \pi^{-1/2} \exp(-\xi^2 r^2) \right. \\ & \left. + \left(\frac{3}{4} r^{-1} - \frac{3}{2} r^{-3} \lambda \right) \text{erfc}(\xi r) \right\} \mathbf{e}_r \mathbf{e}_r, \quad (10) \end{aligned}$$

$$\begin{aligned} \mathbf{M}^{(r,s)}(\mathbf{k}) = & \left(1 - \frac{1}{3} k^2 \lambda \right) \left(1 + \frac{1}{4} \xi^{-2} k^2 + \frac{1}{8} \xi^{-4} k^4 \right) 6\pi k^{-2} \\ & \times \exp\left(-\frac{1}{4} \xi^{-2} k^2\right) (\mathbf{I} - \mathbf{e}_k \mathbf{e}_k). \quad (11) \end{aligned}$$

$\mathbf{M}^{(p,s)}$ is the mobility associated to lattice sum in real space, $\mathbf{M}^{(r,s)}$ concerns with the sum in reciprocal space, $r = |\mathbf{x}_{\gamma\beta} - \mathbf{x}_\alpha|$, $\mathbf{e}_r = \mathbf{r}/r$, $\mathbf{e}_k = \mathbf{k}/k$, $\lambda = \frac{1}{2}(1 + a_p/a_s)$ and erfc is the complementary error function. The mobilities presented from the Eq. (9) to (11) provide two different levels of hydrodynamic interaction approximation. The terms which include λ^2 provide a leading order correction due to the finite size of the particles.

Considering the system under the action of gravity and that the particles are torque-free, the force \mathbf{F}^α acting on a particle α of species s is given by

$$\mathbf{F}^\alpha = -\eta_s \lambda_s^3 \mathbf{e}_3 + \mathbf{f}_l^\alpha + \mathbf{f}_c^\alpha. \quad (12)$$

The term $-\eta_s \lambda_s^3 \mathbf{e}_3$ is the net weight of the particle α and \mathbf{f}_l^α is an artificial short-range repulsive force acting among pairs of particles when they are close together and \mathbf{f}_c^α is a restoring force to prevent eventual overlaps. One discusses short-range interaction next.

For a mobility problem the particle trajectories are obtained simply by integration of the kinematic equation

$$\frac{D\mathbf{x}^\alpha}{Dt} = \mathbf{U}^\alpha, \quad \mathbf{x}^\alpha(0) = \mathbf{x}_0^\alpha. \quad (13)$$

3.2 Short-Range Repulsive Forces. As mentioned above, the mobility tensors include only the far-field interactions which cannot capture the lubrication forces arising from the squeezing

flow within the gap between two approaching spheres. As a consequence, in a time evolution of disordered suspensions it is common the occurrence of numerical errors owing to occasional overlaps between the spheres, even in dilute systems. Such a problem is critical in regions of large solid volume fractions especially when particles have settled at the bottom of the container.

In view of this a lubrication short-range force is modeled here by employing an artificial repulsive force acting among pairs of particles when they are close together, [11]. Introduction of this extra repulsive force to prevent particles clusters is not unrealistic because forces acting between particles in nature and in laboratory practice are often repulsive. Furthermore, the pairwise addition of near-field lubrication forces in Stokesian dynamics simulations of Brady and Bossis [31] requires time steps prohibitively small to prevent overlaps.

The expression for this repulsive force is given by

$$\mathbf{f}_l^\alpha = C_1 \eta_p \lambda_p^3 \exp\left[-\frac{(-\varepsilon_{\alpha\beta})}{\lambda_p C_2}\right] \hat{\mathbf{r}}, \quad \text{for } 0 < (-\varepsilon_{\alpha\beta}) < \varepsilon_0 \quad (14)$$

where C_1 and C_2 are arbitrary numerical parameters which represent, respectively, the intensity and the range of the repulsive force, $\varepsilon_{\alpha\beta} = (\lambda_s + \lambda_p) - |\mathbf{x}_\beta - \mathbf{x}_\alpha|$ is the virtual overlap, and ε_0 is the interparticle gap for which the force \mathbf{f}_l^α is cut off. The parameters C_1 , C_2 , and ε_0 were determined by means of numerical experiments with two unequal sedimenting spheres with an upstream impact parameter of $a_l = \lambda_p a$. Figure 2 presents the time evolution of the gap between two closing unequal spherical particles. The accuracy of the numerical simulation was tested by performing calculations for two interacting particles that have been studied extensively in the past and for which analytical and simulation results are available for comparison, [32]. For a time step (1/100) Stokes time it is found a minimum gap around 1/10 of the particle radius, when imposing the above short-range repulsive force with the appropriate constants C_1 , C_2 , and ε_0 . Typical values for these constants are: $C_1 = 10$, $C_2 = 0.1$, and $\varepsilon_0 = 0.1$.

Although the lubrication forces have a divergent character when the particles come close at the creeping flow regime, it is considered in addition the restoring force \mathbf{f}_c^α due to eventual elastic collisions. For simplicity it was employed a linear force-displacement relation for interparticle contact in such a way that the normal elastic force is proportional to the virtual overlap of the particles, so that

$$\mathbf{f}_c^\alpha = -K_e \varepsilon_{\alpha\beta} \hat{\mathbf{r}}, \quad \text{for } \varepsilon_{\alpha\beta} > 0 \quad (15)$$

where K_e denotes the contact stiffness, assumed to be constant, whose value depends upon material and geometric properties of the colliding spheres. After several tests we found a typical value for this constant equal to 100. Here, the repulsive forces may be also employed to model particle-wall interactions in a system with no flux boundaries parallel to gravity.

3.3 Impenetrable Boundaries. The image system is constructed by considering a unit cell with dimensions $d \times l \times 2h$, being the real and reciprocal lattice vectors defined now as $\mathbf{x}_\gamma = (\gamma_1 d, \gamma_2 l, \gamma_3 2h)$ and $\mathbf{k}_\zeta = 2\pi(\zeta_1/d, \zeta_2/l, \zeta_3/2h)$, respectively, where $\{\gamma_1, \gamma_2, \gamma_3\}$ and $\{\zeta_1, \zeta_2, \zeta_3\}$ are sets of integer coefficients. The procedure to obtain the flow solution within a no flux boundary is essentially to consider a linear combination $\mathbf{u}(\mathbf{x}) = \mathbf{u}(\mathbf{x}; \mathbf{x}_\alpha^s) + \mathbf{u}(\mathbf{x}; \mathbf{x}_\alpha^i)$ satisfying the following boundary conditions:

$$\begin{cases} u(\mathbf{x}), v(\mathbf{x}), w(\mathbf{x}) & \text{periodic in } x \text{ and } y \text{ directions} \\ & \text{with period } d \text{ and } l, \text{ respectively} \\ u(\mathbf{x}), v(\mathbf{x}) & \text{periodic in } z \text{ with period } h \\ w(\mathbf{x}) = 0 & \text{on } z = 0 \text{ and } z = h, \end{cases} \quad (16)$$

where u , v and w denote the components of the fluid velocity. The term $\mathbf{u}(\mathbf{x}; \mathbf{x}_\alpha^s)$ corresponds to the periodic flow solution due to

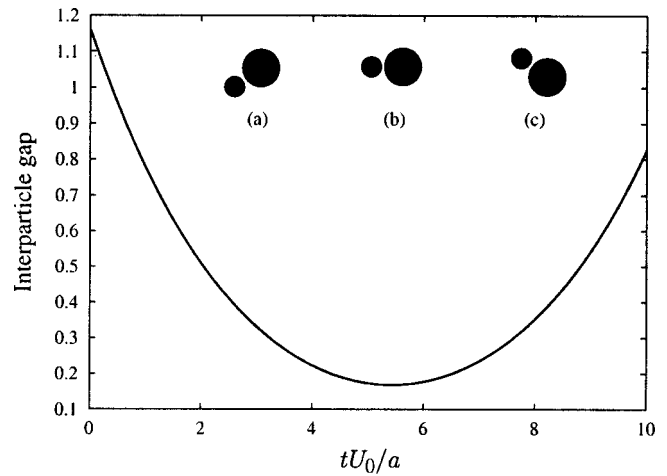


Fig. 2 Time evolution of the dimensionless gap between two unequal sedimenting spheres. The figure is for an aspect ratio of $\lambda_l/\lambda_s = 1.75$ with upstream impact parameter λ_l . In the inset are represented three steps of the time evolution, being (b) the step of minimum interparticle gap.

a stokeslet located at $\mathbf{x}_\alpha^s = (x, y, z)$. The complementary term $\mathbf{u}(\mathbf{x}; \mathbf{x}_\alpha^i)$ corresponds to the image system which consists of a stokeslet equal in magnitude but opposite in sign located at the image point $\mathbf{x}_\alpha^i = (x, y, -z)$, [33].

Using such an image system with Ewald's summation technique in the version of Beenakker [28] we arrive at the fundamental solution for the Stokes flow induced by a lattice of stokeslets with side periodicity and impenetrable top and bottom. The general form for the velocity of a particle α is given by

$$\mathbf{U}^\alpha = \mathbf{M}^\alpha(\xi) \cdot \mathbf{F}^\alpha + \sum_{\beta=1}^N \mathbf{G}(\mathbf{x}_\beta - \mathbf{x}_\alpha, \xi) \cdot \mathbf{F}^\beta, \quad (17)$$

where $\mathbf{G}(\mathbf{x}_\beta - \mathbf{x}_\alpha, \xi)$ is the Ewald summed mobility tensor, given by

$$\mathbf{G}(\mathbf{x}_\beta - \mathbf{x}_\alpha) = \sum_{\substack{\gamma \\ \mathbf{x}_{\gamma\beta} \neq \mathbf{x}_\alpha}} \mathbf{J}^{(ps)}(\mathbf{x}_{\gamma\beta} - \mathbf{x}_\alpha) + \frac{1}{V} \sum_{\substack{\zeta \\ \mathbf{k}_\zeta \neq 0}} \mathbf{M}^{(rs)}(\mathbf{k}_\zeta) \Theta \quad (18)$$

being the kernel tensor $\mathbf{J}^{(ps)}$ and the function Θ defined as

$$\mathbf{J}^{(ps)} = \mathbf{M}^{(ps)}(\mathbf{x}_{\gamma\beta}^s - \mathbf{x}_\alpha, \xi) - \mathbf{M}^{(ps)}(\mathbf{x}_{\gamma\beta}^i - \mathbf{x}_\alpha, \xi), \quad (19)$$

$$\Theta = \cos[\mathbf{k}_\zeta \cdot (\mathbf{x}_\beta^s - \mathbf{x}_\alpha)] - \cos[\mathbf{k}_\zeta \cdot (\mathbf{x}_\beta^i - \mathbf{x}_\alpha)]. \quad (20)$$

The term $\mathbf{M}^{(ps)}$ is the periodic Green's function in the physical space presented in Section 3.1 and the vectors $\mathbf{x}_{\gamma\beta}^s = (x, y, z) + \mathbf{x}_\gamma$ and $\mathbf{x}_{\gamma\beta}^i = (x, y, -z) + \mathbf{x}_\gamma$ locate the source point and the image point, respectively.

4 Numerical Method

Equations (13) and (17) will be applied to examine the dynamics of N particles sedimenting and interacting hydrodynamically within a container with a no flux boundary perpendicular to gravity direction and periodic boundary conditions in the horizontal direction. This type of formulation represents a mobility problem with hydrodynamic interactions, calculated by using pairwise additivity (i.e., superposition of velocity in the mobility matrix). It should be important to note that the moderate number of particles used in the present simulations makes the effect of periodicity dominate the sedimentation velocity at small particle volume frac-

tion, and the relatively low number of multipoles included (i.e., degenerate quadrupole only) reduces the accuracy at high ϕ . Improvements could be made on both fronts by including more multipole on the one hand and more particles on the other. Either of these approaches, however, increases dramatically the number of degrees-of-freedom and results in prohibitive computation times, even avoiding the costly (N^3) inversion from hydrodynamic lubrication. The simulations here requires for the calculation of the mobility interactions $O(N^2)$ operations, which is still excessive at moderate ϕ .

4.1 Sampling Techniques. In this section, we describe a procedure based on the method proposed by Metropolis et al. [34] to simulate the initial condition for either monodisperse and multimodal size distributions of many interacting spherical particles. The main aim of this method is to generate ergodic ensembles in which each member consists of N mutually impenetrable spheres whose centers are randomly distributed in a prismatic unit cell of volume V .

Consider the rigid sphere system defined in Section 3. The mutual impenetrability of the spheres imposes that the center of a test sphere of radius a_s cannot be located within an excluded volume shell $a_p < |\mathbf{r}| < a_p + a_s$ of any other one of radius a_p . In other words, these systems are characterized by a pair potential which is zero when the interparticle distance is greater than $a_p + a_s$ and infinite when $|\mathbf{r}| \leq a_p + a_s$.

In order to simulate a narrow fluid gap separating the spheres when they are in close proximity, a geometric parameter ϵ is incorporated into the excluded volume. The amount of this gap is arbitrary but it is determined by considering the physical phenomenon to be simulated, such as sedimentation or shear flow. This parameter is also considered in order to calibrate numerically the minimum distance between spheres during the generation process. The value of ϵ must be chosen with some care, since it magnifies the exclusion-volume effects, and consequently exerts an important influence upon the randomness degree of the distributions. In terms of the aspect ratios and the mentioned geometric parameter, the numerical excluded volume is written as

$$\lambda_p + \frac{1}{2} \epsilon < |\mathbf{r}| < \lambda_p + \lambda_s + \frac{1}{2} \epsilon \quad (p, s = 1, \dots, m). \quad (21)$$

The generation procedure for a given volume fraction $\phi = (4/3)\pi \sum_{i=1}^m n_i \lambda_i^3$ begins by placing sequentially the required number N of particles within the periodic domain under the non-overlap condition. Increasing ϵ , the impenetrability condition imposes more severe restrictions on available particle arrangements and decreases the physically accessible space.

From the set $C_N = (\mathbf{x}_1, \dots, \mathbf{x}_N)$, which characterizes the static initial configuration of the particles, one attributes to the system a potential energy, defined by

$$E(C_N) = \sum_{\alpha=1}^N \sum_{\beta=\alpha+1}^N \mathcal{V}(r_{\alpha\beta}), \quad (22)$$

where $\mathcal{V}(r_{\alpha\beta})$ is an arbitrary pair potential which falls off rapidly with distance $r_{\alpha\beta} = |\mathbf{x}_\beta - \mathbf{x}_\alpha|$, and gives a weight $P(C_N) = \exp(-E)$, which defines an ergodicity criterion.

The system is subject to a temporal evolution simulated numerically as a random diffusive walk governed by the following Brownian-diffusion equation

$$\mathbf{x}_{n+1} = \mathbf{x}_n + \text{Pe}^{(s)} \delta t + \sqrt{6\lambda_s^{-1} \delta t} \boldsymbol{\varepsilon}_n \quad (23)$$

where $\boldsymbol{\varepsilon}_n$ is a random vector with each component having zero mean and unit variance and being generated independently of the other components and independently of previous time steps. Numerically, this random vector is obtained by means of a standard random number generator with enough independence between adjacent numbers, [35]. During the diffusion simulations the deterministic displacement $\text{Pe}^{(s)} \delta t$ was neglected by the imposition of

$\text{Pe}^{(s)} \ll 1$, which leads to isotropic particle motion. While the system evolves, the impenetrability condition was employed based upon the excluded volume criterion given by Eq. (21), in which ϵ is set to a value representative of the lubrication gap.

The evolution of the system from the initial distribution to subsequent nonoverlapping configurational states, in particular the motion of each particle, is subject to an energy criterion which prescribes: If the movement of a particle α implies in a reduction of the system energy, the new position vector \mathbf{x}_α^{n+1} will integrate into the set C_N by substituting the element \mathbf{x}_α . Otherwise, one considers the energy increment ΔE due to movement and takes a random number ϵ between 0 and 1. The position \mathbf{x}_α^{n+1} will be allowed only if $\epsilon < \exp(-\Delta E)$. In the case in which $\epsilon > \exp(-\Delta E)$, the new position is forbidden and the prescriptions outlined above are similarly followed for the next particle.

4.2 Computation of Hydrodynamic Interactions. To compute hydrodynamic interactions among spherical multisized particles in a semi-dilute ($\phi \leq 0.15$) suspension, one presents a numerical procedure based upon the Ewald summation technique for the Rotne-Prager mobility tensor, [28]. Although the Ewald sum technique overcomes the convergence problems intrinsic to the long-range nature of interparticle interactions, it demands great computational effort which decreases the suitability of the method for large systems. It is the purpose of the method presented below to reduce the computational effort in order to permit a study of some aspects of microstructural dynamics and an evaluation of transport properties based on meaningful statistics. Our computational resource permits the simulation of monodisperse and polydisperse suspensions characterized by N of $O(10^3)$, N being the number of particles in a periodic cell.

The lattice sum computation, in each time step of the temporal evolution, demands $O(n_{pc} N^2)$ computations, n_{pc} being the number of periodic cells in the lattice. A significant computational saving is achieved by tabulating *a priori* the periodic Green's functions (10) and (11) in order to avoid the computation of the mobility tensor during the simulation. This scheme takes advantage of an important feature of the two-sphere mobility, which is a function of the relative separation only. Although the computational effort still scales with N^2 , the avoidance of lattice sum computations reduces drastically (about 98%) the CPU time. However, the computational effort growing with N^2 imposes severe constraints on system size and consequently a number of particles greater than few thousands is prohibitively large for dynamic simulations. A typical number of particles we simulated in a unit cell is 300 for dynamic simulations with 10 realizations, and 1000 for static simulations averaging over a hundred particle configurations. Typically it takes 5–10 s CPU time for the simulation of one time step ($\Delta t = 0.01a/U_0$) on a 933 MHz Dell work station. The maximum memory required for the largest problem and the tabulation process is around 25–100 MB. Recently, Sireou and Brady [36] have described a method for calculating the hydrodynamic interactions among particles in suspension at small Reynolds number based on a Stokesian dynamics method with a reduced computational cost of $O(N \ln N)$. However, the work was limited to evaluation of macroscopic properties of static suspensions (not evolving in time). We should also mention here the existence of $O(N)$ algorithms developed by Ladd [37] and by Mo and Sangani [38]. Ladd's method is based on the lattice-Boltzmann technique for finite Reynolds number of $O(N)$, although he recognizes that there are several possible sources of error in his simulations. Sangani and Mo's algorithm follows a well-known approach by calculating the full resistance matrix through a fast multipole summation technique and inverting the resulting matrix iteratively. This method is in principle $O(N)$, although the iterative solution employed for these authors appears to perform poorly.

5 Numerical Results

We first test the accuracy of the method by comparing sedimentation velocities given by the present simulation with some analytical and experimental results available.

5.1 Hindered Settling Function for Ordered Suspensions.

The first case we consider is a periodic arrangement of spheres sedimenting in a simple cubic lattice. For this case the theoretical hindered settling function scales as $O(\phi^{1/3})$ for point particle force (i.e., dilute limit), [39]. We verify our numerical scheme by comparing calculated sedimentation rates with the asymptotic, low-volume fraction solutions of Sangani and Acrivos [40], given by

$$f(\phi) = 1 - 1.7601\phi^{1/3} + \phi - 1.5593\phi^2 + 3.9799\phi^{8/3} - 3.0734\phi^{10/3} + O(\phi^{11/3}). \quad (24)$$

Figure 3 shows the settling velocity for a simple cubic array of spherical particles as a function of $\phi^{1/3}$. It can be seen that the numerical results, obtained by considering the finite size of the particles, yield close agreement with the theoretical predictions given by Eq. (24) in the semi-dilute particle volume fraction range $\phi \leq 0.20$. It is also displayed the point-particle numerical results in order to illustrate the effect of the level of the hydrodynamic approximation on the sedimentation velocity.

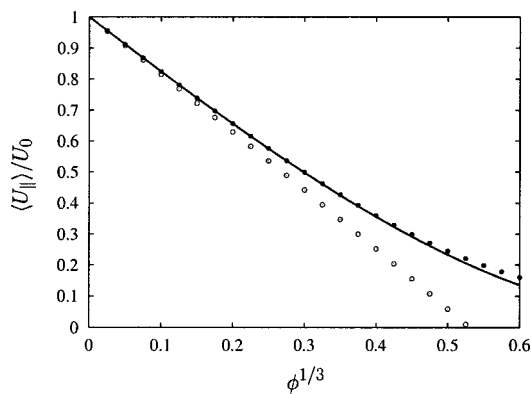


Fig. 3 Dimensionless settling velocity as a function of $\phi^{1/3}$ for a simple cubic arrangement of particles. The numerical results for point-particle approximation (\circ) and including the finite size of the particle (\bullet) are shown in comparison with the low ϕ asymptotic solution of and Sangani-Acrivos [40] (solid curve).

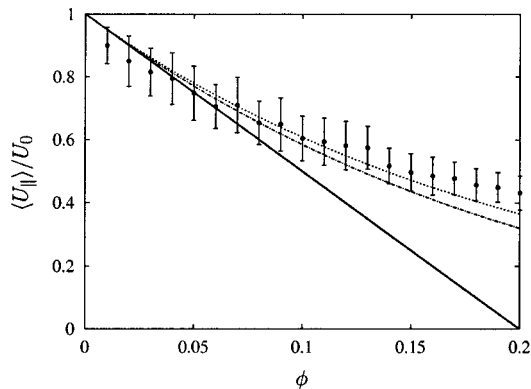


Fig. 4 Dimensionless settling velocity as a function of the solid volume fraction. Simulations results (\bullet) are shown in comparison with the low ϕ asymptotic result of Batchelor [3] (solid curve), the Brady-Durlofsky [41] result (dashed curve) and the Richardson-Zaki correlation [2] (dashed-dotted curve).

5.2 Hindered Settling Function for Disordered Suspensions. The calculation of the settling velocity averaged over several instantaneous random configurations of particles constitutes a more realistic test than the above. In this section we validate the hindered settling function by means of comparisons with Richardson-Zaki [2] correlation,

$$f(\phi) = (1 - \phi)^n, \quad (25)$$

for which we assumed an exponent $n=5.1$, and with the low ϕ asymptotic result of Batchelor [4] for random and statistically homogeneous suspensions, given by

$$\langle U_{||} \rangle / U_0 = f(\phi) \sim 1 - 5\phi + O(\phi^2). \quad (26)$$

It is also made a comparison with the analytical expression of Brady and Durlofsky [41]

$$f(\phi) = \frac{\langle U_{||} \rangle}{U_0} = 1 + \phi - \frac{1}{5}\phi^2 - \frac{6}{5}\phi \left(\frac{5 - \phi + 1/2\phi^2}{1 + 2\phi} \right), \quad (27)$$

derived by considering the Rotne-Prager approximation for the Percus-Yevick hard-sphere radial distribution function, [41].

The instantaneous mean of the velocities of the sedimenting particles is

$$\bar{\mathbf{U}}(t) = \frac{1}{N} \sum_{i=1}^N \mathbf{U}_i(t). \quad (28)$$

Figure 4 shows the results for the dimensionless average sedimentation rate as a function of the particle volume fraction for a random monodisperse suspension together with Eqs. (25) to (27). Each point corresponds to the mean velocity over 100 independent particle configurations at a given concentration. Good accuracy for the sedimentation velocity is obtained for the wide range of particle volume fraction simulated ($0 < \phi < 0.20$). At low volume fraction ($\phi \leq 0.03$), however, the numerical results underpredict Batchelor's theory being the agreement within statistical uncertainty. The small degree of scatter suggests that some of the initial random configurations accessible through our simulations were not perfectly statistically homogeneous as assumed by Batchelor's analysis. Actually, the dilute limit is difficult to study through simulation, as very small effects must be compared and issues of system size, the effect of periodic boundary conditions must be considered. In this limit the motion is in essence a superposition of the sedimentation velocity of the dilute periodic array of images which scales like $(\phi/N)^{1/3}$, with that for the random suspension which is $O(\phi)$ for a low-volume fraction. Mo and Sangani [38] have calculated this difference in the velocity induced at the center of a test particle in a periodic suspension and a random suspension. Experimental results do not seem also to give Batchelor's coefficient, generally giving a value less than 6.55. The hindering of the settling observed is due to a back flow outside the particle, which occurs since we imposed the condition of no mean flow, $\langle \mathbf{u} \rangle = 0$. Our method can predict accurate velocity only for low to moderate volume fractions; for higher volume fractions more moments are required to represent the particles correctly. (See Figs. 5 and 6.)

5.3 Hindered Settling Function for Bidisperse Suspensions

We now present the calculated hindered settling velocities for a bimodal size suspension of equidensity particles. At dilute conditions the comparisons are made with the theoretical result of Batchelor [4] which states that the mean velocity of a particle of species s in a suspension of m distinct species is given by

$$f_s(\phi) = \frac{\langle U_{||}^{(s)} \rangle}{U_0^{(s)}} \sim 1 + \sum_{p=1}^m S_{sp}(\lambda, \eta) \phi_p + O(\phi^2) \quad (s = 1, 2, \dots, m) \quad (29)$$

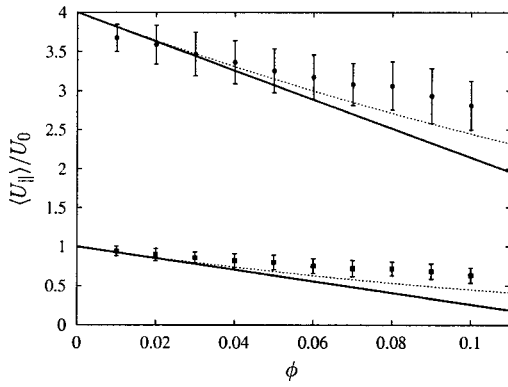


Fig. 5 The settling velocity, nondimensionalized by U_0 , as a function of the total solid volume fraction for a bimodal size suspension. Simulation results for small (\square) and large (\bullet) species are shown in comparison with the low ϕ asymptotic result of Batchelor-Wen [43] (solid curve) and the Davis-Gecol correlation [42] (dashed curve). The simulations were performed over 100 random and equally probable configurations. The system is comprised of 1000 particles in a cubic periodic cell. The results are for $\phi_s = \phi_l = \phi/2$ and $\lambda_l/\lambda_s = 2$.

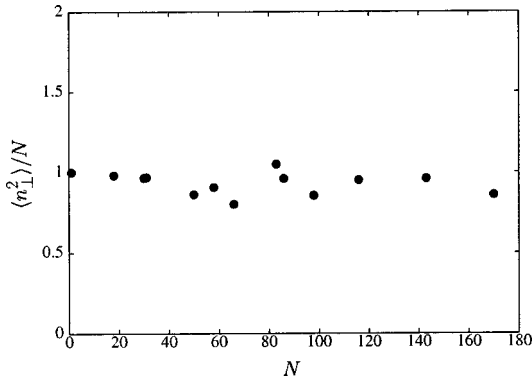


Fig. 6 Dimensionless horizontal density fluctuation obtained over 100 random and independent configurations as a function of the number of particles.

where S_{sp} values are sedimentation coefficients which depend upon the aspect ratio $\lambda = a_p/a_s$ and the reduced density ratio $\eta = (\rho_p - \rho_f)/(\rho_s - \rho_f)$.

As another basis for comparison one adopts the correlation proposed by Davis and Gecol [42], valid for a wider range of total particle volume fraction, given by the following expression:

$$f_s = \frac{\langle U_{\parallel}^{(s)} \rangle}{U_0} = \lambda_s^2 (1 - \phi)^{-S_{ss}} \left(1 + \sum_{p \neq s} (S_{sp} - S_{ss}) \phi_s \right) \quad (30)$$

where the sedimentation coefficients S_{sp} assume the appropriate values calculated by Batchelor and Wen [43].

In Figure 7 it is shown the numerical results for the mean settling velocity as a function of the total particle volume fraction in comparison with those predicted by the Eqs. (29) and (30). For the sedimentation coefficients it was assumed the numerical values $S_{11} = S_{22} = -5$, $S_{12} = -9.81$, $S_{21} = -4.29$ provided by Batchelor and Wen [43]. The simulations were performed under the imposition of equal volume fractions for both particle species. The numerical results were obtained by averaging over 100 random and independent instantaneous configurations. We see that they are in good general agreement with the correlation, [43], thus validating the calculations of the average sedimentation by the present numerical procedure.

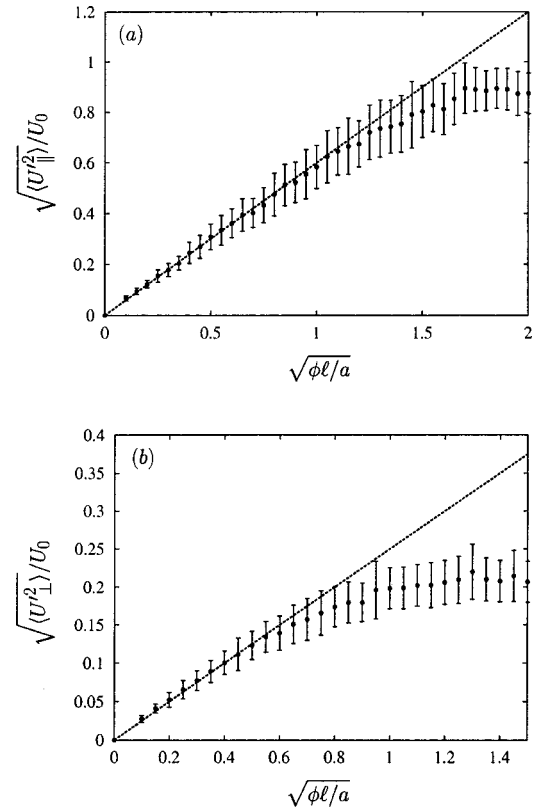


Fig. 7 Dimensionless velocity fluctuation for a monodisperse suspension as a function of the system parameter $\sqrt{\phi l/a}$. The simulations were performed over 100 random and equally probable configurations. The system is comprised of 300 particles in the unit cell with periodic sides and impenetrable boundaries perpendicular to gravity. The dashed lines are the linear fit: (a) $\sqrt{\langle U_{\parallel}^2 \rangle}/U_0 = 0.79 \sqrt{\phi l/a}$; (b) $\sqrt{\langle U_{\perp}^2 \rangle}/U_0 = 0.20 \sqrt{\phi l/a}$.

5.4 Fluctuations in Sedimentation. Several cases were studied. The particle concentration was varied through the range $0 < \phi < 0.10$. Various different box sizes were studied, with l/a ranging from around 25 to 350. The aspect ratio of the box was kept constant at $h/l = 3$.

The horizontal fluctuations in the density of the suspension are the origin of the large convection currents during the sedimentation. We investigate the magnitude of these fluctuations by constructing the Fourier amplitude for the lowest mode in the x -direction of the number density $\langle n_{\perp}^2 \rangle$

$$\langle n_{\perp}^2 \rangle = \sum_{j,k} e^{2\pi i(x_j - x_k)/l}, \quad (31)$$

summing over the differences in the x -coordinates of the positions of the particles.

We collect together in Fig. 6 the average of the horizontal density fluctuations, normalized by N , over the 100 realizations in each of the 12 different cases studied. Although the results are plotted as a function of the number of particles used in the different cases, we see that the horizontal density fluctuations are essentially constant, equal to the standard $\pm \sqrt{N}$ statistical fluctuation. The small degree of scatter around the unit we attribute to the effect of the finite size of the box.

We measure the fluctuations in the velocities with the instantaneous variance

$$\langle U'^2(t) \rangle = \frac{1}{N-1} \sum_{i=1}^N (U_i(t) - \bar{U}(t)), \quad (32)$$

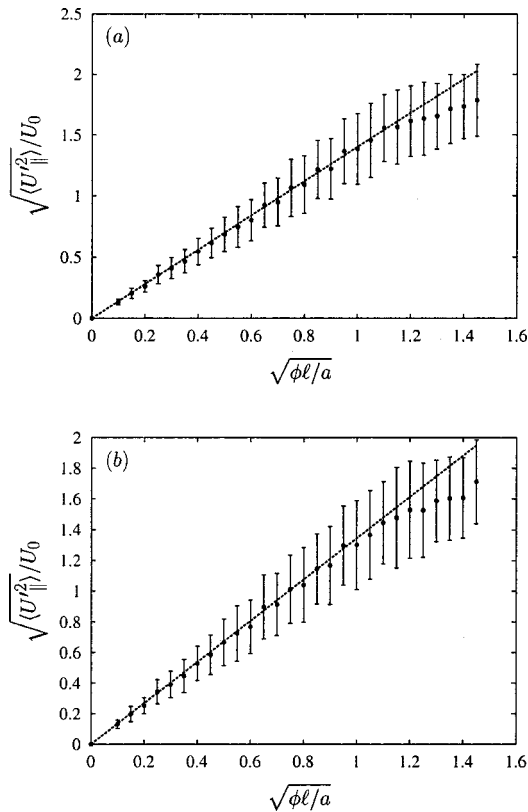


Fig. 8 Dimensionless vertical velocity fluctuation for a bidisperse suspension as a function of the system parameter $\sqrt{\phi l/a}$. The simulations were performed over 100 random configurations. The system is comprised of 300 particles in the unit cell with periodic sides and impenetrable box. The results are for $\phi_s = \phi_l = \phi/2$ and $\lambda_l/\lambda_s = 2$. The dashed lines are the linear fit: (a) $\sqrt{\langle U_{||}^2 \rangle}/U_0 = 1.400\sqrt{\phi l/a}$; (b) $\sqrt{\langle U_{\perp}^2 \rangle}/U_0 = 1.345\sqrt{\phi l/a}$.

constructed for the vertical and two horizontal components of velocity, the variances of the horizontal components then being averaged to give $\langle U_{||}^2 \rangle$ and $\langle U_{\perp}^2 \rangle$.

In Figures 7(a) and 7(b) we examine the variation of the fluctuations in the vertical and horizontal velocities. The system was comprised of 300 particles in a unit cell with no flux boundary perpendicular to gravity, but with side periodicity. The results for the cases with different particle concentrations ϕ and box sizes a/l are plotted against the expected scaling parameter $(\phi l/a)^{1/2}$. We see that for low-volume fractions and small boxes both velocity fluctuations increase linearly with the square root of the box size, with linear fits $\sqrt{\langle U_{||}^2 \rangle} = 0.79U_0(\phi l/a)^{1/2}$ and $\sqrt{\langle U_{\perp}^2 \rangle} = 0.20U_0(\phi l/a)^{1/2}$. Thus in agreement with Cafisch and Luke [7] and with the scaling argument presented here, we conclude that when the particles are positioned randomly in a monodisperse dilute suspension there are initially variances proportional to the size of the box.

The saturation of the velocity fluctuations in Figs. 7(a) and 7(b) are obtained for a volume fraction around 0.19 and l/a 18.7. It is seen that velocity fluctuations parallel to gravity reach the constant value of $0.85U_0$ for $(\phi l/a)^{1/2}$ around 1.5, whereas the velocity fluctuations perpendicular to gravity reach the value $0.20U_0$ for $(\phi l/a)^{1/2}$ around 0.8. The velocity fluctuation of the vertical velocity is comparable to the mean sedimentation velocity. This is in good general agreement with the experiments [23] where the fluctuations ranged between 25% and 50% of the mean in the dilute suspensions. Our results are also in good general agreement with the experiments of Nicolai et al. [25] and Guazzelli [6] who found a relative fluctuation around 80% at $\phi = 5\%$. The theoret-

ical value of Koch and Shaqfeh [9] gives a slightly higher value of $\sqrt{\langle U_{||}^2 \rangle} = 2.2U_0$. The ratio in Fig. 7 of the vertical to horizontal velocity fluctuations was found to be 4, indicating a strong anisotropy. This is near to the experiment value of 2.5 found by Nicolai et al. [25] and Guazzelli [6], and near to the ratio of 3.5 found by theory and numerical simulations, [14–16].

We next present simulation results for a bidisperse suspension. These simulations were performed for equal concentration of the large and the small species ($\phi_s = \phi_l = \phi/2$) and for a diameter ratio 2. Figures 8(a) and 8(b) display the results for vertical velocity fluctuations for two species as a function of the system parameter $(\phi l/a)^{1/2}$. It is seen that the hydrodynamic interactions of small particles with larger ones produces an increasing in their velocity fluctuations of about 30% compared to the results shown in Fig. 7(a). It is apparent from these results that random bidisperse suspensions present a system size dependence at low-volume fraction, just as shown above for the monodisperse case. This leaves open the possibility that a dilute homogeneous polydisperse suspension could exhibit hydrodynamic screening.

5.5 Suspension Evolution. Microstructural change, that is the variations in the relative arrangements of the particles, is an important feature of a sedimentation process. The time evolution of the system was analyzed over 10–20 realizations. The main problem that we examine was to know how the initial configurations of the particles evolve in time.

Typical evolutions for the cases of monodisperse and bimodal suspensions simulated are displayed in Fig. 9. Figure 9(a) shows one realization of the monodisperse case for a particle concentration $\phi = 5\%$, a box size of $l/a = 20$ and an aspect ratio of the box $h/l = 3$; a simulation requiring 286 particles. The realization of the bimodal suspension is shown in Fig. 9(b) for $l/a = 20$, a total concentration $\phi = 0.05$ ($N = 185$), $\phi_s = \phi_l = 0.025$, and aspect ratio $\lambda_l/\lambda_s = 1.5$ and $h/l = 3$. We show at five different times (from 0 to $60 a/U_0$) the positions of the particles projected onto the vertical xz -plane. The first time in both cases is the initial configuration with the particle distributed randomly inside the box. As time progresses, a sediment accumulates on the lower impen-

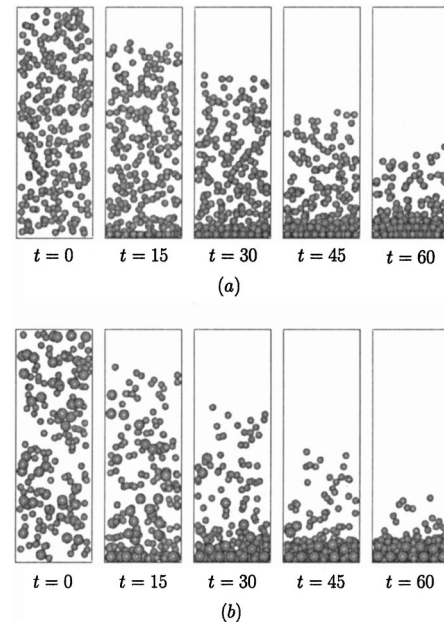


Fig. 9 Typical dynamic simulation of particle configuration at different times during sedimentation: (a) monodisperse sedimentation for $a/l=0.05$, $h/l=3$, $N=286$; $\phi=0.05$; (b) bimodal sedimentation for $\phi=0.05$ ($N=185$), $\phi_s = \phi_l = 0.025$ and aspect ratio $\lambda_l/\lambda_s = 1.5$; $h/l=3$.

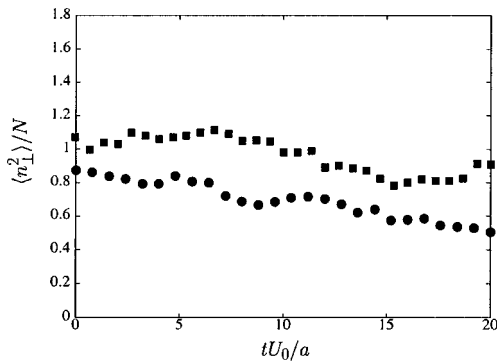


Fig. 10 Time evolution of the dimensionless horizontal density number fluctuations at different conditions of the simulated system with the aspect ratio $h/l=3$. (\square): $a/l=0.05$; $\phi=0.03$ ($N=172$), (\bullet): $a/l=0.06$; $\phi=0.02$ ($N=66$).

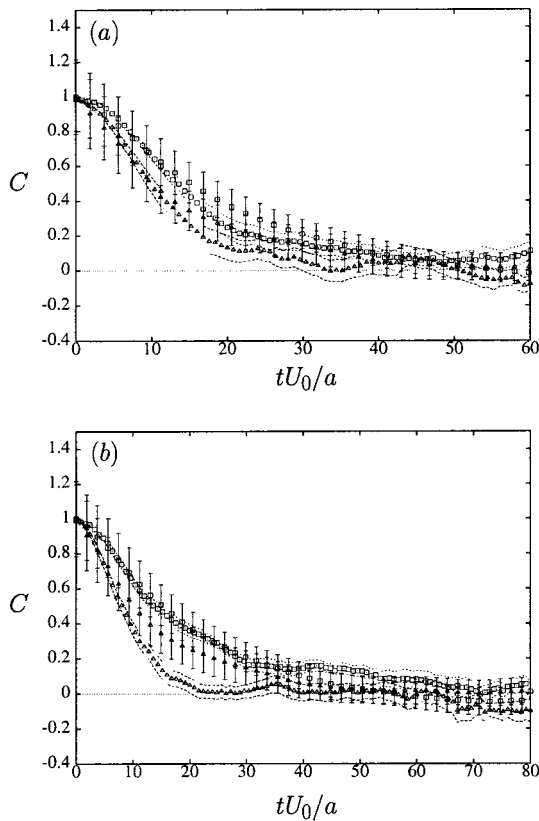


Fig. 11 Normalized velocity fluctuation auto-correlation functions parallel, C_{\parallel} (\square) and perpendicular, C_{\perp} (Δ) to the gravity direction. (a) Computer simulations for $h/l=3$, $a/l=0.05$, $N=114 \Rightarrow \phi=0.02$; (b) Computer simulations for $h/l=3$, $a/l=0.05$, $N=172 \Rightarrow \phi=0.03$. The error bars represent experimental data [25] with $\phi=0.05$, $h/l=4$, $h/d=10$ and $d/a \approx 100$. The dashed lines indicate the uncertainly range of the present computer simulations.

etrable boundary. Note that the impenetrable boundary is slippery and not a no-slip rigid boundary, so that particles can be seen moving along it. The descending upper interface between the suspension and clear fluid above is diffuse and spreads slowly, so that the nearby concentration of particles decreases in time.

For each case studied, dynamic simulations were made for 10 to 20 realizations with different initial configurations. Below we give only averages over these realizations. Moreover in calculat-

ing the averages, we select the middle part of the suspension, away from the sediment and the diffuse upper front.

Variations in number density can result from different boundary conditions, such as when a finite height of suspension settles toward an impenetrable plane boundary as considered in our simulations. Figure 10 shows the time evolution of the horizontal density fluctuations, normalized by N , for two different combinations of particle concentrations and box size. In each of the two different cases studied, the horizontal density fluctuations are seen to remain essentially constant up to $t=20a/U_0$, approximately the time to fall through the width of the box l or one third the time to fall the height of the box h . We had expected that during such a time the density fluctuations would drive a convection which would turn the horizontal variations in density into vertical variations, and so the large velocity fluctuations would decay. Our dynamic simulations show, however, that the convection does not lead to a systematic decrease in the horizontal density fluctuations. Further simulations, [11], with a taller box, $h/l=4$ and $h/l=5$ found the same behavior. This result indicates that, even in the case of considering no flux slip boundaries one would not expect the probability density in the bulk of the suspension to be influenced. Thus, the fluctuations seem to be always limited by the box size in the dilute limit of a sedimenting suspension.

Corresponding to the lack of evolution of the density fluctuations, vertical velocity fluctuations therefore remain proportional to the size of the box, as in the parameter $\phi l/a$, and do not evolve to some value which is independent of the size of the box. The computer simulations therefore remain at variance with experimental observations of fluctuations independent of the size of the box. A possible explanation to the discrepancy between experiment and theory is that side walls in the experiments may induce large inhomogeneities as the suspension evolves in time. Furthermore, the experiments are always affected by polydispersity at low-volume fraction. Polydispersity could decrease the correlation time for a particle allowing it to fall through the interaction volume faster than it can sample the same volume by hydrodynamic dispersion. This effect would be important to decrease diffusivity as observed in the experiments.

The velocities of the particles fluctuate randomly in time, apparently with a magnitude which does not evolve during the sedimentation. The persistence in time of the velocity fluctuations is investigated using the auto-correlation function of the velocity fluctuations, which correlates the velocity at time t with itself at various time delays τ . This is constructed for the vertical and two horizontal components. We shall report these auto-correlation functions normalized by the variances, i.e.,

$$C_{\parallel}(t) = \frac{\langle U'(t)U'(t+\tau) \rangle}{\langle U'(t)U'(t) \rangle} \quad (33)$$

and similarly for $C_{\perp}(t)$. Here the angle brackets denote a sum over all particles, and an average over all configurations or realizations (i.e., an average over time in dynamic simulation).

Figure 11 gives the auto-correlation function, nondimensionalized by the variance (correlation with zero time delay), for the horizontal and vertical velocity, both for our computer simulations in the case $\phi=3\%$, $a/l=0.05$ and $h/l=3$ and for the experiments of Nicolai et al. [25] in the case $\phi=5\%$, $a/l=0.01$, $h/l=10$, and $l/d=2.5$. There is good general agreement in which the velocities lose correlation over a time of $O(10a/U_0)$ and the horizontal velocity de-correlates slightly faster.

The random motion of the sedimenting particles can be characterized by a diffusion process with diffusivity calculated as the integral over time of the velocity auto-correlation function

$$D = \int_0^{\infty} \langle U'(t)U'(t+\tau) \rangle dt, \quad (34)$$

constructed for the vertical D_{\parallel} and averaged over the two horizontal directions for D_{\perp} .

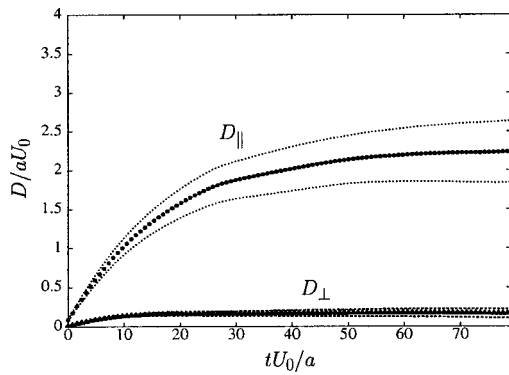


Fig. 12 Dimensionless hydrodynamic self-diffusivities for $h/l = 3$, $a/l = 0.05$, and $\phi = 3\%$. The dashed lines are the error bars.

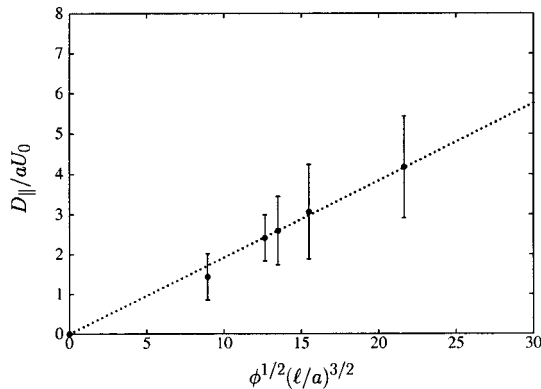


Fig. 13 Vertical dimensionless hydrodynamic self-diffusivity as a function of the scaling $\phi^{1/2}(l/a)^{3/2}$. The dot line is the linear fit $D_{\parallel} = 0.19aU_0\phi^{1/2}(l/a)^{3/2}$.

$$\mathbf{D} = \mathbf{e}_z \mathbf{e}_z D_{\parallel} + (\mathbf{I} - \mathbf{e}_z \mathbf{e}_z) D_{\perp} \quad (35)$$

An important question is to examine whether this integral converges at long times: if it does not, the diffusion process is anomalous. The ratio of the diffusivities to the velocity variance gives the integral time-correlation $D/\langle U'^2 \rangle$.

Figure 12 shows the time integral increasing to its asymptotic value on the correlation time of $O(10a/U_0)$. For the case $\phi = 3\%$, $a/l = 0.05$ and $h/l = 3$ we find a diffusivity in the direction of gravity $D_{\parallel} = 2aU_0$. This value should be compared with the experimental values of Ham and Homsy [23] increasing from $2aU_0$ at $\phi = 2.5\%$ to $6aU_0$ at $\phi = 6\%$, and the experimental value of Nicolai et al. [25] around $5aU_s$. Hydrodynamic screening theory gives $D_{\parallel} = 0.52aU_0/\phi$, i.e., the larger value $17aU_s$ at $\phi = 3\%$, [9].

Figure 13 shows our results for the self-diffusivity parallel to gravity as a function of the scaling parameter $\phi^{1/2}(l/a)^{3/2}$. The results for various particle concentrations ϕ and box sizes a/l can be approximated by the linear fit $D_{\parallel} = 0.19aU_0\phi^{1/2}(l/a)^{3/2}$. While the values of the diffusivity are comparable with those in laboratory experiments, a direct comparison is not possible because our simulations depend on the size of the box and the laboratory experiments do not.

The random fluctuations during sedimentation exhibit considerable anisotropy. We find that $D_{\parallel}/D_{\perp} \approx 10$ in all our simulations. This value should be compared with a value around 5 in the experiments of Nicolai et al. [25], and a value around 25 in the theory of Koch [14]. In fact, Koch's theory shows that it is possible to reduce a degree of anisotropy from 100 to around 25 by increasing the aspect ratio of the box from $h/l = 1$ to $h/l = 3$. We speculate, however, that this still high value results from the use

of a full periodic boundary condition in the vertical rather than our no flux boundary perpendicular to gravity. Ladd [16] reported numerical results of fluctuations and hydrodynamic dispersion in sedimentation for a large homogeneous suspension using 32768 particles ($\phi = 10\%$) at finite Reynolds number ($Re = 0.45$), based on the width of the periodic cell. His results show an anisotropy in velocity fluctuations about 3 that agree well with our numerical results and experiments. However, the ratio of diffusivities equal to 24 for $h/l = 4$ are larger than the result here and about five times the experimental measurements.

Finally, we consider the results for velocity fluctuation fields across the whole box at $\phi = 0.03$. The simulations show how the random initial structure develops in time. Figure 14 displays typical velocity fluctuation fields taken during the dynamical simulation at time t from 0 to $75a/U_0$. The starting time ($t = 0$) corresponds to a random suspension generated as described in Section 4.1. It is apparent that coherent large-scale structure that are order of the size of the box forms (convective currents of particles) and persists at later times. This larger scale vortex structure indicates that the velocity fluctuations depend on the system size.

From the above discussion it seems as though that simulations with a finite height of suspension approaching a no-flux boundary with periodic boundary conditions in the horizontal direction is the key to better capture the anisotropic nature of the particle interactions and also to understand the difference between theory and experiments on dilute sedimenting suspensions. This problem can be better explored through simulations considering a box with no-slip boundaries in order to investigate the effect of the container walls on the dynamic of fluctuations as particles sediment.

6 Conclusions

In this paper we report direct numerical simulations of mono-disperse and polydisperse suspensions of spherical particles sedimenting at low Reynolds number in a rectangular container with side periodicity and impenetrable slip boundaries perpendicular to gravity. Our method is applicable for static (not developing in time) and dynamic simulations of suspensions at moderately low volume fractions. The method of images was peculiarly adapted to the solution of the problem of many interacting particles. The results show the importance of including the effect of a no-flux lower boundary for reducing the vertical-horizontal anisotropy of particle diffusivities to realistic proportions.

We have compared our results of sedimentation velocity for ordered and random (monodisperse and polydisperse) suspensions with theory and experimental correlations and have generally found good agreement for particle volume fraction ranging from 0 to 0.20. It is seen that the sedimentation velocities do not agree particularly well in the very dilute limit due to the effect of periodicity of our numerical system. For higher volume fractions a good agreement of our sedimentation with experiments would require higher-order many-body multipole moments.

The results also show the evolution of the positions of the particles in a finite box. Our numerical computations have found velocity fluctuations of monodisperse and polydisperse dilute suspensions increasing in a predictable way with the system size. It is seen that a saturation of fluctuations occurs only at volume fractions larger than 10%. This result agrees with the scaling arguments presented here, with theory and with large-scale lattice-Boltzmann simulations of dilute suspensions. We conclude that the sedimentation process observed in our simulations has been dominated by convection currents (large structure motion) of the size of the settling box, which is preserved in time. In contrast, the experiments have found that large vortex structures diminishes in size at larger times.

The degree of anisotropy in velocity fluctuations and hydrodynamic self-diffusivities, both experimentally and in the present simulations are independent of the system size. Our simulation results for normalized autocorrelation functions are also in good agreement with experiments at dilute limit.

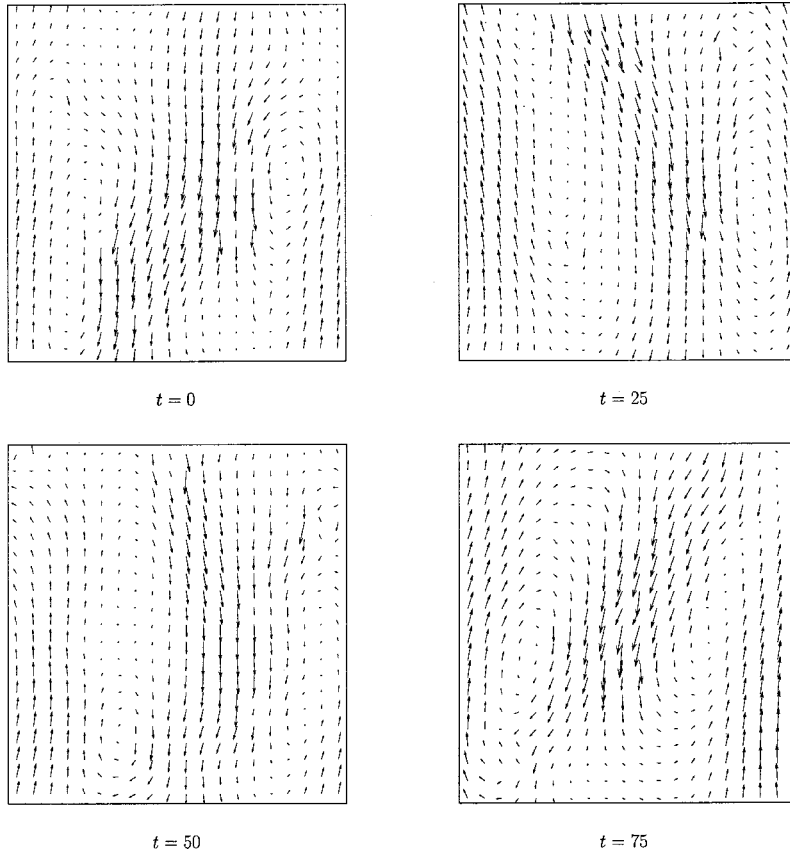


Fig. 14 Time developing of three-dimensional velocity-fluctuation fields across the numerical box ($20 \times 20 \times 60$) during the sedimentation process of monodisperse particles at $\phi = 0.05$. The dimensionless time corresponds to multiples of Stokes time a/U_0 . Large-scale motions (i.e., convective currents) dominate the sedimentation process with large swirl depending on the numerical box.

Since the experimental systems are never perfectly homogeneous and the actual particle distribution is unknown, the experimental observations have not a definite answer for the physical mechanism that renormalizes the rms fluctuations in a dilute sedimenting suspension. Certainly new numerical simulations including the effects of the container walls would be important and challenging to explain the experimental observations.

We hope that our simulations have given some new insights into the study of fluctuations and dispersion in sedimentation and may help to stimulate new developments in the future.

Acknowledgments

We acknowledge the support from CNPq-Brasil and Finep-CTPETRO. We wish to thank Elizabeth Guazzelli (LPMH/ESPCI, Paris) for kindly providing the experimental data plotted in Fig. 11.

Nomenclature

a = particle radius
 C = velocity autocorrelation function
 C_1, C_2 = numerical parameters (see Eq. (14))
 D = hydrodynamic self-diffusivity
 D_0 = Stokes-Einstein diffusivity
 d = box width
 \mathbf{F} = force acting on the particles
 \mathbf{f}_l^{α} = artificial lubrication force acting on a particle α
 \mathbf{f}_c^{α} = artificial contact force acting on a particle α
 $f(\phi)$ = hindered settling function

\mathbf{G} = Ewald summed mobility tensor
 \mathbf{g} = gravitational force per unit mass
 h = box height
 \mathbf{I} = unit second-rank tensor
 \mathbf{J} = kernel tensor
 K_c = contact stiffness
 \mathbf{k}_ζ = reciprocal lattice vector
 l = box length
 \mathbf{M} = mobility tensor
 m = number of species
 N = number of particles within the unit cell
 n = number density of particles
 Pe = Péclet number
 \mathbf{r} = relative distance vector
 Re = Reynolds number
 $S(\lambda, \eta)$ = sedimentation coefficients
 St = Stokes number
 U_0 = Stokes velocity
 U' = particle velocity fluctuation
 u, v, w = fluid velocity components
 V = cell volume
 \mathbf{x} = position vector
 \mathbf{x}_γ = physical lattice vector
 x, y, z = space coordinates

Greek Symbols

γ = cell index of the physical lattice
 ΔE = energy variation
 $\Delta \rho$ = particle-fluid density difference

- δt = time step
- ϵ = geometric parameter (see Eq. (21))
- ϵ_n = random vector
- ϵ_0 = interparticle gap for which the force \mathbf{f}_i^α is cut off
- $\epsilon_{\alpha\beta}$ = virtual overlap between particles α and β
- ζ = cell index of the reciprocal lattice
- η = reduced density ratio
- κ = Boltzmann constant
- λ = aspect ratio
- μ = fluid viscosity
- ξ = convergence parameter
- ρ = particle density
- ρ_f = fluid density
- τ_c = correlation time
- ϕ = solid volume fraction

Superscripts

- α, β = particle index
- (ps) = physical space
- (rs) = reciprocal space
- (s), (p) = given species

Subscripts

- \parallel = parallel to gravity
- \perp = perpendicular to gravity
- s = small species
- s, p = given species
- l = large species

References

- [1] Davis, R. H., and Acrivos, A., 1985, "Sedimentation of Noncolloidal Particles at Low Reynolds Number," *Annu. Rev. Fluid Mech.*, **17**(91), pp. 91–118.
- [2] Richardson, J. F., and Zaki, W. N., 1954, "Sedimentation and Fluidization: I," *Trans. Inst. Chem. Eng.*, **32**(35), pp. 35–52.
- [3] Batchelor, G. K., 1972, "Sedimentation in a Dilute Dispersion of Spheres," *J. Fluid Mech.*, **52**, pp. 245–268.
- [4] Batchelor, G. K., 1982, "Sedimentation in a Dilute Polydisperse System of Interacting Spheres. Part 1. General Theory," *J. Fluid Mech.*, **119**, pp. 379–408.
- [5] Davis, R. H., 1996, "Hydrodynamic Diffusion of Suspended Particles: A Symposium," *J. Fluid Mech.*, **310**, pp. 325–335.
- [6] Guazzelli, E., 2001, "Evolution of Particle-Velocity Correlations in Sedimentation," *Phys. Fluids*, **13**(6), pp. 1537–1540.
- [7] Caffisch, R. E., and Luke, J. H. C., 1985, "Variance in the Sedimentation Speed of a Suspension," *Phys. Fluids*, **28**(3), pp. 759–760.
- [8] Hinch, E. J., 1988, *Disorder and Mixing*, Kluwer Academic, Dordrecht, pp. 153–161, Chap. 9.
- [9] Koch, D. L., and Shaqfeh, E. S. G., 1991, "Screening in Sedimenting Suspensions," *J. Fluid Mech.*, **224**, pp. 275–303.
- [10] Koch, D. L., 1992, "Anomalous Diffusion of Momentum in a Dilute Gas-Solid Suspension," *Phys. Fluids*, **4**(7), pp. 1337–1346.
- [11] Cunha, F. R., 1995, "Hydrodynamic Dispersion in Suspensions," Ph.D. Thesis, Department of Applied Mathematics and Theoretical Physics, Cambridge University, Cambridge, UK.
- [12] Cunha, F. R., 1997, "On the Fluctuations in a Random Suspension of Sedimenting Particles," *J. Braz. Soc. Mech. Sci.*, **19**(4), pp. 474–495.
- [13] Brenner, M. P., 1999, "Screening Mechanisms in Sedimentation," *Phys. Fluids*, **11**(4), pp. 754–772.
- [14] Koch, D. L., 1994, "Hydrodynamic Diffusion in a Suspension of Sedimenting Point Particles With Periodic Boundary Conditions," *Phys. Fluids*, **6**(9), pp. 2894–2900.
- [15] Ladd, A. J. C., 1993, "Dynamical Simulation of Sedimenting Spheres," *Phys. Fluids*, **5**(2), pp. 299–310.
- [16] Ladd, A. J. C., 1997, "Sedimentation of Homogeneous Suspensions of Non-Brownian Spheres," *Phys. Fluids*, **9**(3), pp. 491–499.
- [17] Cunha, F. R., Rosa, O. S., and Sousa, A. J., 2001, "Do We Understand Hydrodynamic Dispersion in Sedimenting Suspensions?" *J. Braz. Soc. Mech. Sci.*, **23**(4), pp. 379–399.
- [18] Nicolai, H., and Guazzelli, E., 1995, "Effect of the Vessel Size on the Hydrodynamic Diffusion of Sedimenting Spheres," *Phys. Fluids*, **7**(1), pp. 3–5.
- [19] Ségre, P. N., Herbolzheimer, E., and Chaikin, P. M., 1997, "Long-Range Correlations in Sedimentation," *Phys. Rev. Lett.*, **79**(13), pp. 2574–2577.
- [20] Kalthoff, W., Schwarzer, S., Ristow, G. et al., 1996, "On the Application of a Novel Algorithm to Hydrodynamic Diffusion and Velocity Fluctuations in Sedimenting Systems," *Int. J. Mod. Phys. C*, **7**(4), pp. 543–561.
- [21] Davis, R. H., and Hassen, M. A., 1988, "Spreading of the Interface at the Top of a Slightly Polydisperse Sedimenting Suspension," *J. Fluid Mech.*, **196**, pp. 107–134.
- [22] Lee, S., Jang, J., Choi, C., and Lee, T., 1992, "Combined Effect of Sedimentation Velocity Fluctuation and Self-Sharpening on Interface Broadening," *Phys. Fluids*, **4**(12), p. 2601–2606.
- [23] Ham, J. M., and Homsy, G. M., 1988, "Hindered Settling and Hydrodynamic Dispersion in Quiescent Sedimenting Suspensions," *Int. J. Multiphase Flow*, **14**(5), pp. 533–546.
- [24] Xue, J.-Z., Herbolzheimer, E., Rutgers, M. A., Russel, W. B., and Chaikin, P. M., 1992, "Diffusion, Dispersion, and Settling of Hard Spheres," *Phys. Rev. Lett.*, **69**(11), pp. 1715–1718.
- [25] Nicolai, H., Herzhaft, B., Hinch, E. J., Oger, L., and Guazzelli, E., 1995, "Particle Velocity Fluctuations and Hydrodynamic Self-Diffusion of Sedimenting Non-Brownian Spheres," *Phys. Fluids*, **7**(1), pp. 12–23.
- [26] Cunha, F. R., and Hinch, E. J., 1996, "Shear-Induced Dispersion in a Dilute Suspension of Rough Spheres," *J. Fluid Mech.*, **309**, pp. 211–223.
- [27] Leighton, D. T., and Acrivos, A., 1987, "The Shear-Induced Migration of Particles in Concentrated Suspensions," *J. Fluid Mech.*, **181**, pp. 415–439.
- [28] Beenakker, C. W. J., 1986, "Ewald Sum of the Rotne-Prager Tensor," *J. Chem. Phys.*, **85**(3), pp. 1581–1582.
- [29] Nijboer, B. R. A., and De Wette, F. W., 1957, "On the Calculation of Lattice Sums," *Physica*, **23**, pp. 309–321.
- [30] Rotne, J., and Prager, S., 1969, "Variational Treatment of Hydrodynamic Interaction in Polymers," *J. Chem. Phys.*, **50**(11), pp. 4831–4837.
- [31] Brady, J. F., and Bossis, G., 1988, "Stokesian Dynamics," *Annu. Rev. Fluid Mech.*, **20**, pp. 111–157.
- [32] Kim, S., and Karrila, S. J., 1991, *Microhydrodynamics: Principles and Selected Applications*, Butterworth-Heinemann.
- [33] Blake, J. R., 1971, "A Note on the Image System for a Stokeslet in a No-Slip Boundary," *Proc. Cambridge Philos. Soc.*, **70**, pp. 303–310.
- [34] Metropolis, N., Rosenbluth, A. W., Rosenbluth, M. N., Teller, A. H., and Teller, E., 1953, "Equation of State Calculations by Fast Computing Machines," *J. Chem. Phys.*, **21**(6), pp. 1087–1092.
- [35] Press, W. H., Teukolsky, S. A., Vetterling, W. T., and Flannery, B. P., 1992, *Numerical Recipes in Fortran 77*, **1**, Cambridge University Press, Cambridge, UK.
- [36] Sierou, A., and Brady, J. F., 2001, "Accelerated Stokesian Dynamics Simulations" *J. Fluid Mech.*, **448**, pp. 115–146.
- [37] Ladd, A. J. C., 1994, "Numerical Simulations of Particulate Suspensions via a Discretized Boltzmann Equation. Part 2. Numerical Results," *J. Fluid Mech.*, **271**, pp. 311–339.
- [38] Mo, G., and Sangani, A. S., 1994, "A Method for Computing Stokes Flow Interactions Among Spherical Objects and Its Application to Suspensions of Drops and Porous Particles," *Phys. Fluids*, **6**(5), pp. 1637–1652.
- [39] Saffman, P. G., 1973, "On the Settling Speed of Free and Fixed Suspensions," *Stud. Appl. Math.*, **52**(2), pp. 115–127.
- [40] Sangani, A. S., and Acrivos, A., 1982, "Slow Flow Through a Periodic Array of Spheres," *Int. J. Multiphase Flow*, **8**(4), pp. 343–360.
- [41] Brady, J. F., and Durlofsky, L. J., 1988, "The Sedimentation Rate of Disordered Suspensions," *Phys. Fluids*, **31**(4), pp. 717–727.
- [42] Davis, R. H., and Gecol, H., 1994, "Hindered Settling Function with No Empirical Parameters for Polydisperse Suspensions," *AIChE J.*, **40**(3), pp. 570–575.
- [43] Batchelor, G. K., and Wen, C. S., 1982, "Sedimentation in a Dilute Polydisperse System of Interacting Spheres. Part 2. Numerical Results," *J. Fluid Mech.*, **124**, pp. 495–528.